Click-based porous cationic polymers for enhanced carbon dioxide capture

Click-based porous cationic polymers for enhanced carbon dioxide capture

by

Alessandro Dani, Valentina Crocellà, Claudio Magistris, Valentina Santoro, Jiayin Yuan and Silvia Bordiga

J. Mater. Chem. A, 2017, 5, 372-383

DOI: 10.1039/C6TA08574A

Click-Based Porous Cationic Polymers for Enhanced Carbon Dioxide Capture

Alessandro Dani,*[a,b] Valentina Crocellà,[b] Claudio Magistris,[C] Valentina Santoro,[d] Jiayin Yuan,[a] Silvia Bordiga*[b]

[a] *A Department of Colloid Chemistry, Max Planck Institute of Colloids and Interfaces Am Mühlenberg 1 OT Golm, D-14476 Potsdam, Germany. E-mail: alessandro.dani@mpikg.mpg.de*
[b] *Department of Chemistry, NIS and INSTM Reference Centre, University of Turin, Via Quarello 15, 10135 Torino, Italy. E-mail: silvia.bordiga@unito.it*
[c] *Department of Chemistry and NIS Interdepartmental Centre, University of Turin, Via P. Giuria 7, 10125 Torino, Italy.*
[d] *Department of Molecular Biotechnology and Health Science, University of Turin, Via Nizza 52, 10126 Torino, Italy.*

Imidazolium based porous cationic polymers were synthesized using an innovative and facile approach, which takes advantage of the Debus-Radziszewski reaction to obtain meso-/microporous polymers following click-chemistry principles. In the obtained set of materials, click based-porous cationic polymers have the same cationic backbone whereas they bear the commonly used anions of imidazolium poly(ionic liquid)s. These materials show hierarchical porosity and good specific surface area. Furthermore, their chemical structure was extensively characterized using ATR-FTIR and SS-NMR spectroscopies, and HR-MS. These polymers show good performance towards carbon dioxide sorption, especially those possessing the acetate anion. This polymer can uptake 2 mmol/g of CO_2 at 1 bar and 273 K, a value which is among the highest recorded for imidazolium poly(ionic liquid)s. These polymers were also modified in order to introduce N-heterocyclic carbene along the backbone. Carbon dioxide loading in the carbene containing polymer is in the same range of the non-modified versions, but the nature of the interaction is substantially different. Combined use of *in-situ* FTIR spectroscopy and micro-calorimetry evidenced a chemisorption phenomenon that brings to the formation of an imidazolium carboxylate zwitterion.

Introduction

Porous organic polymers are a well-established among the field of porous materials.[1-5] More than ten years of research allowed for the discovery of many materials that differ in structure, porosity, functional groups crystallinity, and long-range order. Extensive research for tuning of these properties leads to target-specific porous polymers, useful to meet a variety of applications, such as gas or molecule storage,[6-8] separation, drug delivery,[9] electronics,[10, 11] and catalysis.[12, 13] Most of these materials are rich in phenyl and alkyne moieties,[14, 15] while only some of them possess ionic groups.[7, 16] One of the promising goals in the field of porous polymers is to introduce task-specific functional groups in the chemical structure of the porous network and target the topology and the structure of the material to a well-defined application.[1, 17] The synthetic pathways for these materials are usually time-demanding and require noble metal-based catalysts, since the common approaches involve Suzuki, Sonogashira-Hagihara cross-coupling and Yamamoto-type Ullmann cross-coupling reactions.[18] In recent years, "click-chemistry" has been exploited for the development of these materials, leading to advantageous and competitive syntheses in terms of time and costs.[19-23] A current challenge for porous polymers is to build up new structures, taking advantage of facile synthetic strategies, e.g. click chemistry-based ones, to transfer functional moieties into the polymers to define relevant industrial applications.

Among various kinds of porous polymers, poly(ionic liquid)s (PILs) are gaining more and more interest over the past years because of the high density of ionic liquid species in the macromolecular architecture, which lead to a broad range of applications.[24-29] Usually porous PILs are synthesized in a bottom-up approach via common radical polymerization, using cross-linker monomers and/or templates.[30-33] Some recent works describe the introduction of imidazolium or pyridinium ionic liquid functionalities inside a microporous polymer, basically by synthesis of different imidazolium or pyridinium functionalized monomers, which are respectively connected together by tetrahedral building unit, using different palladium based cross-coupling catalysis.[12, 13, 16, 34] Furthermore, two other groups reported about the closure of the imidazolium ring during the formation of the polymer network, in a two-step reaction. In this case the first step was the synthesis of the Schiff base polymer network; once the material was isolated, the imidazolium ring was closed in a second step.[7, 35]

In this work we describe how to obtain a set of "click-chemistry" based imidazolium porous poly(ionic liquid)s. These porous cationic polymers are obtained taking advantage of modified Debus-

Radziszewski imidazolium synthesis, which follows the main principles of the "click-chemistry" defined by Sharpless *et al.*[36, 37] The Debus-Radziszewski reaction for the production of imidazole dates back to more than a century ago,[38, 39] because of the high yield and the very mild conditions, this reaction remains the benchmark for industrial imidazole production.[40] A modified version of this reaction developed by Esposito *et al.* allows for the direct synthesis of imidazolium ionic liquids. This reaction already proved efficienct towards the synthesis of amino acid-derived imidazolium ionic liquids, linear poly(ionic liquid)s, and to cross-link polymers with dangling amino groups.[41-43] Its efficiency was also proven starting from aromatic amine and aldehyde as reactants.[44, 45]

Herein we exploited the Debus-Radziszewski imidazolium synthesis for the homocondensation of tetrakis(4-aminophenyl)methane, one of the most common tetrahedral building units used for the synthesis of microporous polymers. This click reaction leads to a network that expands in all the three dimensions, and the intrinsic steric hindrance of the monomers confers porosity to the resulting polymer. The reaction is irreversible because of the covalent closure of the thermodynamically stable imidazolium ring and runs under kinetic rather than thermodynamic control; therefore the resulting material is amorphous in nature. The as-obtained polymeric architecture faces the imidazolium cation linked through the position 1 and 3 to the main chain, differing from the common PILs that bear imidazolium as dangling groups. This imidazolium main chain polymeric architecture was described only in few works and showed increased thermal stability of the polymer and different chemical properties arising from the conjugation of the imidazolium with two phenyl rings.[46, 47]

Ionic liquids and poly(ionic liquid)s are well known materials for carbon dioxide adsorption.[48-50] We would like to take both the advantages of their intrinsic affinity towards this molecule and transfer it in microporous polymers, which are already known for their good gas adsorption properties.[51] The as-synthesized click reaction-based porous cationic polymers (from hereafter referred to as CB-PCPs) shows one of the highest carbon dioxide adsorption capacities ever reported among porous PILs, 2 mmol/g at 273K and 1 bar. CB-PCPs are imidazolium functionalized porous polymers, obtained *via* facile click-synthesis, and bearing all the common anions used in the field of PILs for carbon dioxide adsorption. N-heterocyclic carbenes (NHC) Are introduced in CB-PCPs, and the microporosity is tuned by varying the synthetic parameters. This set of CB-PCPs permit to understand how carbon dioxide adsorption properties are related to the structure and the porosity of the materials. In addition a deep physico-chemical study, performed with *in-situ* FTIR spectroscopy and adsorption micro-calorimetry, allows one to distinguish different interactions between carbon dioxide onto ionic polymers, or onto NHC bearing polymers.

Syntheses

Click reaction-based porous cationic polymers (CB-PCPs) were synthesized according to the procedure reported in Scheme 1. Briefly, tetrakis(4-aminophenyl)methane was dissolved in a mixture of water and acetic acid. In a second vial, formaldehyde and methyl glyoxal were dissolved in water and acetic acid. These two solutions were mixed together and the reaction proceeded immediately, as evidenced by solution color variation from yellow to dark brown, due to the development of the conjugated aromatic system; then the solution was heated at 80 °C for 12 hours (Scheme 1 part a) to complete the reaction. The acetic acid is used as catalyst and also ended up as acetate anion in the final product, named CB-PCP **1.** The proposed mechanism of modified Debus-Radziszewski imidazolium synthesis is repored in Figure S1. Others CB-PCPs having different anions are obtained by anion exchange of CB-PCP **1** polymer solution with different salts. We used sodium tetrafluoroborate, bis(trifluoromethane)sulfonimide lithium salt, potassium hexafluorophosphate, and sodium trifluoromethanesulfonate to obtain respectively CB-PCP **2**, **3**, **4** and **5** (Scheme 1, part b). NHC was introduced by reacting polymer CB-PCP **1** with potassium *tert*-butoxide in anhydrous THF for 72 hours; the obtained sample is named CB-PCP **6** (Scheme 1, part c). All the polymers were purified according to their physical aggregation status: if in solution, they were dialyzed against water; if as a gel they were washed with water. Finally, powdery CB-PCPs **1**-**5** were obtained by freeze-drying, whereas moisture-sensitive CB-PCPs **6** was washed with anhydrous solvent and freeze-dried from 1,4-dioxane. Detailed description of syntheses can be found in the supporting information. A successful anion exchange offers an indirect evidence of the successful closure of the imidazolium ring during the synthesis. In fact, only a cationic polymer is able to permanently bind various anions along the structure, without their leaching during the washing step. This new click-based synthetic approach makes PCPs and porous PILs even more green and sustainable.[19] The main strengths of this reaction route are the following:

- It leads to high yield of the final polymer (almost 100%).
- It only forms water as sub-product.
- It has a high thermodynamic driving force arising from the closure of the imidazolium ring.
- Reaction products are stable and the reaction is not reversible.
- 85% Efficiency in atomic economy is obtained.[52]
- Reaction takes place in very mild conditions (80 °C for 12 hours).
- Reagents are easily available except for the tetra-amine, which requires some synthetic steps.
- Reaction uses water and acetic acid as solvents.
- Final products are solids (CB-PCPs **1a**, **1b**, **2-5**) and they are easily purified from the residual monomers by washing with water.

The modified Debus-Radziszewski reaction itself works at room temperature and is rather fast (about 1 hour) when performed at a molecular level or in the case of linear polymers.[41, 42] On the contrary, in the case of cross-linked polymer, it is necessary to increase both temperature and reaction time due to the higher viscosity.

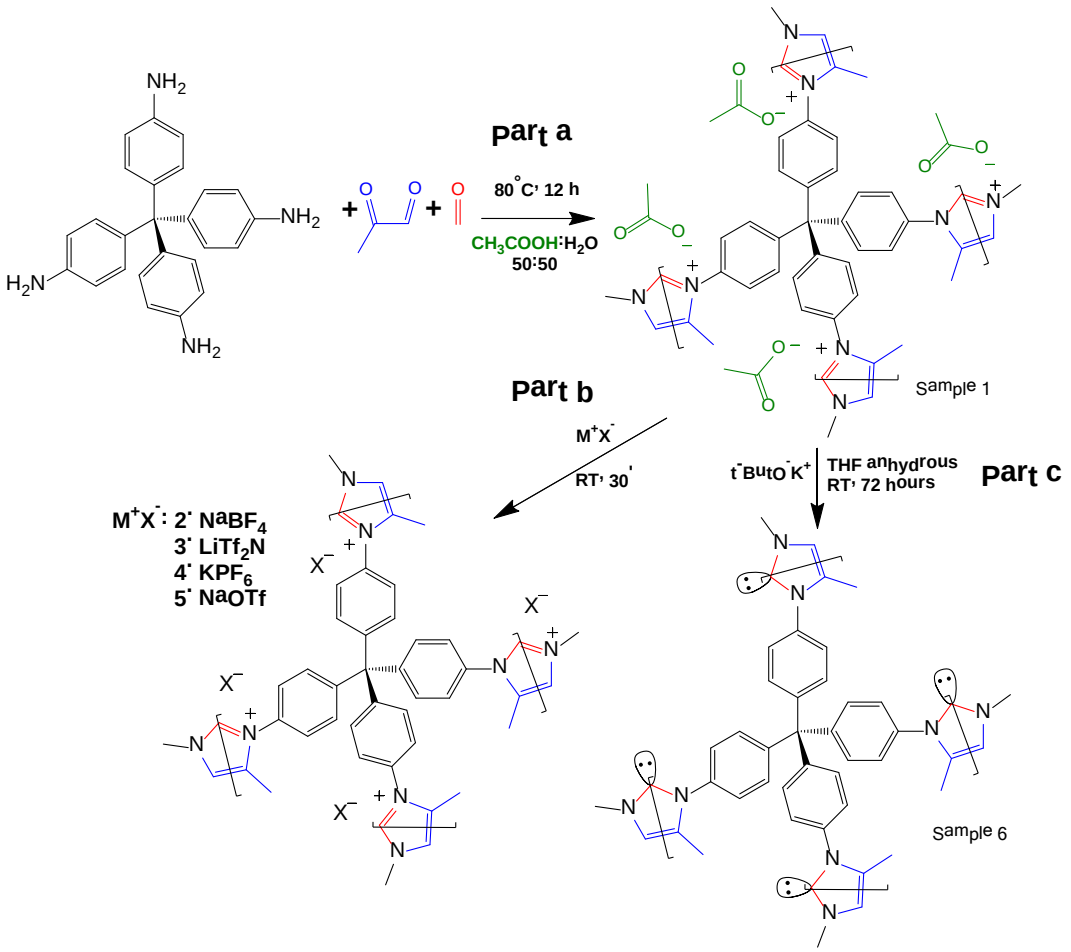

Scheme 1. **Part a:** the synthetic route towards the sample CB-PCP 1 starting from thetetrakis(4-aminophenyl)methane in a one-step reaction. **Part b:** the anion exchange towards the samples CB-PCP **2**, **3**, **4** and **5**. **Part c:** the synthetic route towards sample CB-PCP 6 introducing NHC from the imidazolium ring.

1.1.1. *Vibrational properties of CB-PCPs*

The attenuated total reflection-infrared (ATR-IR) spectrum of sample **1**, reported in Figure 1 curve b, was collected as the first evidence of the successful polymerization. The spectrum is characterized by a series of complex overlapped absorptions. In particular, the two bands located at 1504 and 811 cm^{-1} can be ascribed to the ν(C=C) stretching of the conjugated aromatic system and to the τ(C-H) out of plane bending respectively.[53] These bands are also well evident in the spectrum of tetrakis(4-aminophenyl)methane monomer, reported as reference in Figure 1 curve a. The first, clear evidence of the occurred polymerization is the absence, in the spectrum of the CB-PCP, of the two peaked signals at 3156 and 3395 cm^{-1} related to the ν(N-H) stretching modes of the amino groups of the monomer. In fact, in the 3500- 3000 cm^{-1} region, only a broad and ill-defined band is present, ascribable to the ν(O-H) stretching vibrations of physisorbed water. Unfortunately, the peculiar absorption band of the imidazolium ring, at around 1160 cm^{-1}, appears too weak to be detectable, due to the presence of the broad set of signals in the 1500-800 cm^{-1} spectral range. For this reason, this specific absorption cannot be used as evidence of the successful polymerization. The band at 1705 cm^{-1} is ascribable to the ν(C=O) stretching mode of the amide moiety of the chain terminals, generated by the reaction between the amino groups of the monomer and the excess of acetic acid. This chemical behavior is also well evident in the mass spectra of the dimer reported herein later. Both the symmetric and antisymmetric stretching modes of the acetate anion can be observed in the spectrum of sample **1,** at 1409 and 1566 cm^{-1} respectively.[54] These bands well evident also in the spectrum of sodium acetate, reported as reference in Figure 1 curve c.

The anion exchange with various salts was performed, as previously described, in order to replace the acetate anion and to obtain a set of different CB-PCPs. The ATR-IR spectra of all these materials were reported in Figure 2 and compared with the spectra of the corresponding salts. In all cases, the vibrational modes of the polymeric network are clearly overlapped with the spectral features of the employed anion. In particular, the following can be observed:

i. The ATR-IR spectrum of sample **2** (Figure 2 curve a) displays a medium broad band at 1060 cm^{-1}, assigned to the asymmetric vibrational modes of the BF_4^- anion,[55]

and a signal at around 3152 cm^{-1}, overlapped with the broad band of physisorbed water, due to the combination of the imidazolium ring stretching mode with the BF_4^- stretching vibrations.[56, 57] The reference spectrum of $NaBF_4$ (Figure 2 curve b) exhibits a single band at 1005 cm^{-1} related to the BF_4^- vibrational modes and this signal is red-shifted with respect to sample **2** due to the strong force field of Na^+ cation interacting with BF_4^-.

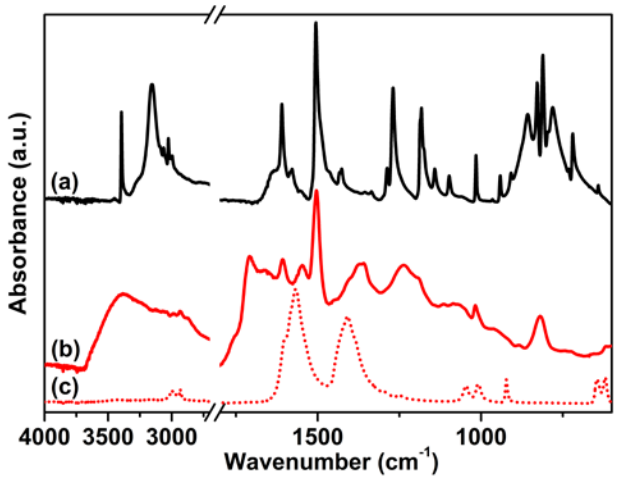

Figure 1. ATR-IR spectra collected in air of tetrakis(4-aminophenyl)methane (a), sample **1** (b) and sodium acetate (c).

ii. In the case of sample **3** the ATR-IR spectrum (Figure 2 curve c) exhibits all the Tf_2N^- ion peculiar vibrational modes (see asterisks) at 747 cm^{-1} (ν(S-N)), 798 cm^{-1} ((ν(C-S)+ν(S-N)), 1188 cm^{-1} (ν(CF_3)) and 1356 cm^{-1} (ν(SO_3))[58], overlapped with that of the polymer network, as highlighted by the comparison with the reference $LiTf_2N$ spectrum (Figure 2 curve d).

iii. A strong band at 841 cm^{-1}, due to the ν(P-F) stretching mode of the PF_6^- anion, is evident in the ATR-IR spectrum of sample **4** (Figure 2 curve e). In the KPF_6 reference spectrum (Figure 2 curve f), this band is red-shifted to 805 cm^{-1} due to the interaction between the ion pairs. In fact, the strong force field of the small K^+ cation affects the length of the P-F bonds of the PF_6^- anion.

iv. Sample **5** presents, in its ATR-IR spectrum (Figure 2 curve g), three new intense bands at 1245 cm^{-1}, 1153 and 1027 cm^{-1} ascribable to the ν(CF_3) and ν(SO_3) modes characteristic of TfO^- anion, as proved by the comparison with the reference spectrum of NaOTf reported in Figure 2 curve h. [59]

The NHC formation in Sample **6** is pointed out by the appearance of a new strong adsorption band at 1605 cm^{-1}, arising from the stretching of the NHC ring (Figure 2 curve i).[7]

Elemental analysis

The elemental analysis of sample **1** was performed in order to obtain quantitative information on the elemental structure of the material. The percentage of C, H and N, reported in Table S1, are respectively 74.78%, 5.55% and 9.11%. These values are in perfect agreement with the calculated ones, pointing out a polymer structure having an elemental compostion corresponding to the suggested structure.

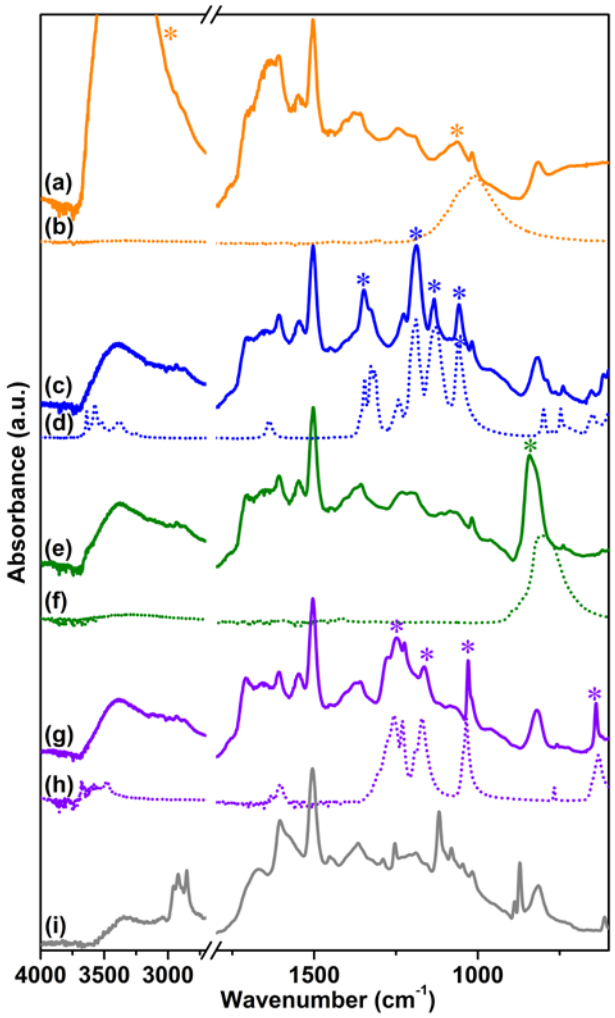

Figure 2. ATR-IR spectra collected in air of sample **2** (a), $NaBF_4$ (b), sample **3** (c), $LiTf_2N$ (d), sample **4** (e), KPF_6 (f), sample **5** (g), NaOTf (h) and sample **6** (i). Starred bands (*) in polymers 1-5 were assigned to anions.

Solid state NMR

In order to prove the structure of CB-PCP 1 and the presence of the imidazolium inside the polymeric network, ^1H (Magic Angle Spinning) MAS and ^{13}C Cross Polarization Magic Angle Spinning (CP-MAS) solid state NMR spectroscopy measurements were performed. Figure 3a shows the ^1H MAS solid state NMR of sample 1 in which two families of protons are clearly distinguishable. The one at lower chemical shift is related to the $-CH_3$ protons of the dangling methyl group in position 4 on the imidazolium ring and also to the $-CH_3$ protons of the acetate anion, whereas the other one is related to the aromatic protons along the polymeric backbone. Figure 3b and c report respectively the ^{13}C CPMAS solid state NMR spectra and a polymer scheme with the corresponding assignations. In the 100-150 ppm range, the carbons constituting the phenyl and the imidazolium rings are well evident.

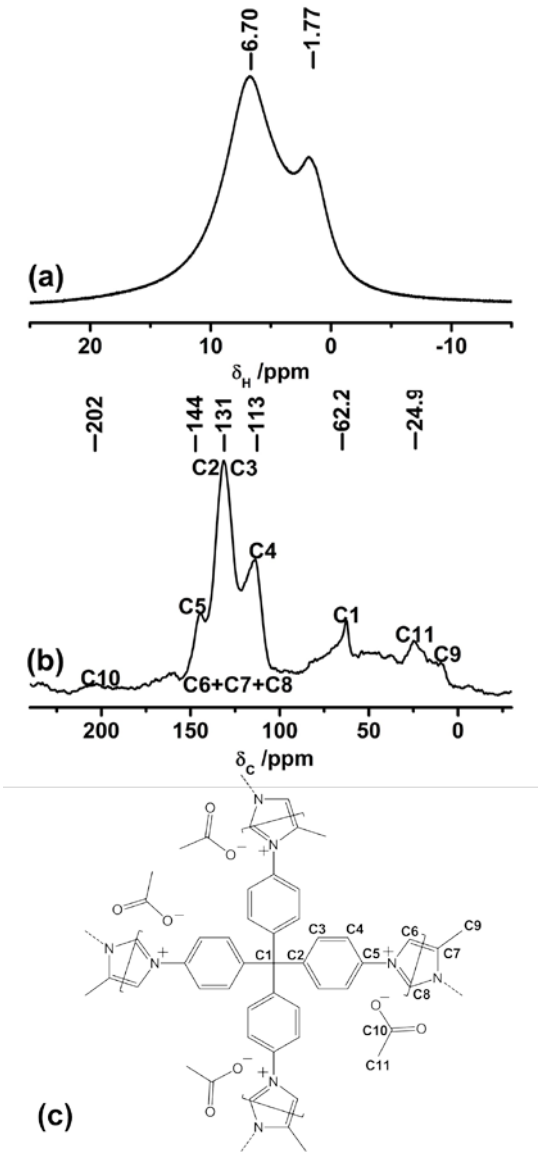

Figure 3. ^{1}H MAS (a) and ^{13}C CP-MAS (b) solid state NMR spectra of sample **1**. (c) scheme of sample **1** that evidence the assignment of ^{13}C CP-MAS spectrum signals.

Three bands are well distinguishable in Figure 3b; however, a specific assignment is not possible due to the overlap between the signals of the phenyl ring and the imidazolium ring carbons. In particular, the band at 62 ppm is related to the quaternary carbon C1**,** the signal at 24.9 ppm is ascribed to the methyl groups carbons C11 and C9, whereasthe ^{13}C carbonyl signal C10 of the acetate anion is visible as a small and broad band at around 200 ppm. It is worth noticing that the main inconvenience to be avoided during the synthesis of **CB-PCP-1** is the formation of a polyimine network, in which the closure of the imidazolium ring by formaldehyde is not fully performed. In this specific case, two ^{13}C strong bands between 150 and 200 ppm, related to imine (C=N) ^{13}C should be present, as reported by Thiel *et al*. [83] **CB-PCP-1** ^{13}C CP-MAS solid state NMR spectrum does not show the two bands related to the imine moiety, indicating the successful formation of the imidazolium network. The weak band at 160 ppm can be ascribable to the acetamide moiety present at the chain terminal.[60]

High resolution Mass spectroscopy

Since sample **1** is obtained in solution after the reaction, we tried to confirm the structure by means of high resolution mass spectroscopy (HR-MS).[61] Unfortunately, the mass weight of the crosslinked polymeric chain of the sample was too high and the electrospray ionization (ESI) failed to transfer the sample from the solution to the gas phase. Therefore we synthesized a partially linear polymer (sample **1s)**, using a lower ratio of aldehydes in respect to the amino monomer (details about this synthesis are reported in the supporting information section), and analysed the reaction solution using HR-MS. From the HR-MS spectra reported in Figure S2**,** it is evident, in the reaction solution, the presence of the dimer having an *m/z* ratio of 809.4156 and, furthermore, a distribution of species ascribable to the dimer bearing the acetamide moiety on the amino groups can be observed (Table S2). The formation of the acetamide moiety is induced by the presence of an excess of acetic acid in solution that reacts with the free amino group of the dimer. Trimer and tetramer formed during the reaction are also visible in the HR-MS spectra (Figure S3 and S4), along with their distribution bearing the acetamide moiety on the amino group (Table S3 and S4), proving the growth of the polymeric chain. Polymeric chains longer than tetramer are difficult to be observed because of the high molecular weight, which prevents the de-solvation and the ionization operated by the ESI source.

Further evidences of the closure of the imidazolium ring are furnished by the MS^n fragmentation obtained for the dimer having an *m/z* ratio of 809.4156, which is reported, together with the purposed chemical structure, in Figure S5 part a-d. The fragmentation shows the loss of the four phenylamino groups, the first two in form of radicals, and the second ones in form of aniline. The imidazolium ring is not fragmented as it is the strongest part of the molecule due to the system of conjugated bonds. The MS^n fragmentation is also performed on the dimer with one acetamide moiety (m/z of 851.4181 shown in Figure S6), highlighting both the losses of free phenylamino group, and phenylamino group with the acetamide moiety. These two signals exhibit different intensities due to statistical distribution.

1.1.2. *Textural and morphological properties of CB-PCPs*

The pore structure of CB-PCPs were investigated by means of N_2 adsorption at 77 K. The adsorption isotherms for sample **1** to **6** are reported in Figure 4. All the isotherms possess a characteristic behavior, already observed in the case of other polymeric networks.[62, 63] More in detail, the adsorption isotherms of samples **1-5** exhibit a pronounced knee at low relative pressuresindicating the presence of

micropores, and, moreover, the isotherm profile constantly rises after the micropores filling, not reaching a plateau. Still,a peculiar hysteresis, in which the desorption branch of the isotherm does not close to the adsorption branch at low relative pressures, can be observed for all the polymers. These phenomena, particularly evident for samples **3**, **4** and **6**, are mostly attributed to a swelling of the polymeric matrix due to the elastic deformations occurring during nitrogen adsorption. [62, 63] For all these reasons, the porosity of these materials is better described by the desorption branches of the isotherms. In fact, being the swelling of the materials proportional to the gas pressure, a fraction of pores is available for N_2 adsorption only at high values of relative pressure. [62, 63] For sample **2**, the desorption branch exhibits a weak step at 0.5 p/p_0, typical of materials with slit pores, whereas,in the case of samples **1** and **5,** the hysteresis is less evident than for the other polymers. These differences probably derive from the various anions, which can slow down the swelling of the material operated by N_2 during the adsorption step.

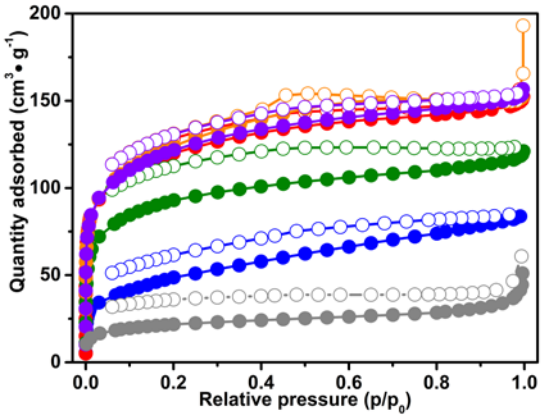

Figure 4. N_2 adsorption isotherms at 77K for samples: **1** (red curve), **2** (orange curve) **3** (blue curve), **4** (green curve), **5** (violet curve) and **6** (dark grey curve).

The Brunauer-Emmett-Teller (BET) specific surface areas (SSAs) of the different CB-PCPs are reported in Table 1. The microporosity of these materials arises from the inefficient packing of the sterically hindered tecton monomers that induces empty spaces inside the network and therefore high accessibility to the formed imidazolium moieties. A fraction of mesopores is also present, deriving from the fragmentation of the network. Since the adsorption isotherms exhibit a mixed behaviour, typical of both mesoporous and microporous materials, the value of BET and Langmuir SSAare both reported in Table 1. In all the materials having the same polymeric backbone, the SSA strongly depends on the anions nature. Sample **1**, **2** and **5**, having hydrophilic anions, exhibit the highest SSAs, probably due to the higher capacity of swelling in aqueous solution that leads to a better retaining of the porous structure during the freeze-drying process. On the contrary, samples **3** and **4**, with hydrophobic anions swell less when suspended in water and after the freeze drying procedure. In fact, they show less porosity as the polymeric chain are more entangled. Sample **6,** the CB-PCP bearing carbene, exhibits a remarkably lower SSA (BET = 77 m^2/g) even if its isotherm retains the profile described for the other materials, pointing out its micro/mesoporous character. The decrease of the SSA is probably ascribable to a partial Wanzlick equilibrium occouring during the carbene synthesis, which leads carbenes to couple each other. [64] Furthermore, the different solvent employed to freeze-drying this material (1,4-dioxane) could confer different swelling properties to the polymeric chains.

Table 1. BET and Langmuir specific surface area of sample **1** to **6** and **1a**, **1b**.

sample name	SSA BET (m^2/g)	SSA Langmuir (m^2/g)	V_{total}[a] (cm^3/g)	V_{micro}[b] (cm^3/g)
1	419	570	0.203	0.131
2	436	595	0.187	0.109
3	176	245	0.109	0.034
4	325	441	0.146	0.088
5	426	578	0.187	0.112
6	77	105	0.055	0.013
1a	396	530	0.128	0.120
1b	8.7	12.9	-	-

[a] Total pore volume obtained from NL-DFT analysis of the adsorption isotherm.
[b] Micropore volume obtained from NL-DFT analysis of the adsorption isotherm.

The pore volume was derived from the adsorption branches of the isotherms, using the non-local density functional theory (NL-DFT) pore model for carbon with slit pore geometry. The total pore volume is around 0.19 cm^3/g for samples bearing hydrophilic anions (*i.e.* sample **1**, **2** and **5**) while it is lower for samples with inferior surface area. The percentage ratio between the micropore volume and the total pore volume is approximately constant (~60%) for all the samples, except for sample **3** which presents a lower ratio (~30%). This behavior can be ascribed to the steric hindrance of the large, hydrophobic Tf_2N^- anion, which can occlude a fraction of the micropores. The total pores volume is lower for sample **6** due to its lower SSA, and it has also a low micropore/total pore volume ratio (~24%), probably due to the increased crosslinking density arising from coupling of carbenes.

In order to investigate the effect of the starting solution concentration on the textural properties of the resulting materials, samples **1a** and **1b** have been synthesized employing solutions two or four times more concentrated respectively (synthesis details are reported in supporting information). The N_2 adsorption/desorption isotherms of these samples are shown in Figure S7, whereas the values of SSA and pores volume are reported in Table 1. The BET SSA of sample **1a** is very similar to the value reported for sample **1** (396 m^2/g), however this material is almost totally microporous. This behavior could derive from the polymer gelification that can occur employing a lower reaction solution volume. The decrease of the available reaction volume induces a reduced swell of the polymer that, in turn, is balanced by the steric repulsion of the tecton monomers, producing an extensive polymeric network mainly constituted of micropores. The further lower reaction

volume of sample **1b,** generates a bulky polymer with an almost null SSA (Figure S7). The pore size distribution plots of all samples are reported in Figure S8 and S9.

The samples morphology was investigated by SEM. Representative SEM images of sample **1** are reported in Figure 5 and in Figure S10 (lower magnification). The CB-PCP **1** appears in form of particles of 1-20 µm. The particles are irregular in shape with evident fragmentation, clearly visible in Figure 5. The microporous structure of these polymers is instead not visible with SEM. The hierarchical porosity in CB-PCPs allows an easy diffusion of gas molecules inside the polymeric matrix thus reaching the imidazolium active sites. SEM images of the other CB-PCPs are not reported, being these materials morphologically very similar to sample **1**.

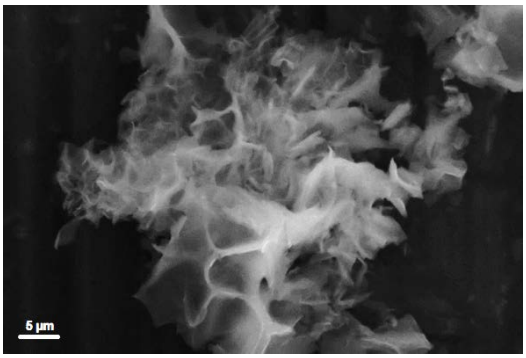

Figure 5. SEM picture of sample **1.**

1.1.3. *Thermogravimetric analysis*

The thermogravimetric analysis of the CB-PCPs **1** to **5** samples are reported in Figure S11. All the thermogravimetric curves are similar despite the different anions, showing a drastic step of weight loss starting at around 400°C related to the decomposition of the polymeric network. The decomposition step is not sharp, probably due to the irregular structure of the network, which broadens the thermal energies range at which the polymer chains break. The materials also exhibit one small weight-loss step starting at 110°C, ascribable to the removal of residual moisture. It is worth noticing that the thermal degradation of the CB-PCPs does not depend on the anion nature. This behavior highlights that the thermal degradation pathway is not the de-alkylation of the imidazolium nitrogen, as observed for dangling imidazolium PILs, but rather the decomposition of the whole polymeric network in one step.

1.1.4. *Carbon dioxide adsorption on CB-PCPs*

The presence of the imidazolium ionic liquid moiety, well known to strongly interact with the CO_2 molecule, together with a microporous network, makes CB-PCPs promising materials for CO_2 capturing. For this reason, a series of volumetric adsorption measurements up to 1 bar and at different temperatures have been performed on the obtained CB-PCPs. Adsorption and desorption isotherms, recorded at 298 K for samples **1**-**6**, are reported in Figure 6. All samples exhibit the peculiar hysteresis observed also for the N_2 adsorption at 77K, in which the desorption branch of the isotherm does not close to the adsorption branch even at low relative pressures. The CO_2 uptake at 298 K and 1 bar is between 1 and 1.2 mmol/g for all the materials. In particular, sample **1** shows the highest loading with a value of 1.2 mmol/g, whereas sample **3** shows the lowest loading of 0.9 mmol/g. The most pronounced hysteresis, observed in the case of sample **3,** can be ascribable to the steric hindrance of the large, hydrophobic Tf_2N^- anion that limits the access of the CO_2 to the imidazolium moiety. Anyhow, all samples show a complete release of CO_2 at room temperature. It is worth noticing that all the CO_2 adsorption isotherms of these samplesdo not reach a plateau at 1 bar. This feature encourage further studies at higher pressures, extending the interest of these materials to the pre-combustion CO_2 capture.[51]

The CO_2 uptake was also evaluated for sample **1** at 273 K and 313 K. The isotherms reported in Figure S12 highlight only a slight decrease of the adsorption capacity at 313 K with a maximum loading of 0.95 mmol/g, on the contrary, at 273 K, the performance of the material drastically improves, almost doubling the maximum loading to a value of 2.05 mmol/g. To the best of our knowledge, this value attests the herein described CB-PCPs as the most performant CO_2 adsorbent materials in the field of the imidazolium PILs. All the previous studies involving PILs for CO_2 adsorption are listed in an extensive review from Zulfigar *et al.*, which encompass PILs with imidazolium, pyridinium or tetraalkylammonium cation and a variety of anions.[48] According to this review, the best CO_2 adsorption capacity at 1 bar and 273 K (0.46 mmol/g) was measured in the case of a cross-linked mesoporous imidazolium PILs obtained by silica hard-templating pathway ($P(SVImTf_2N)$).[65] In the field of porous imidazolium polymers, it is remarkable the work reported by Zhao *et al.* in which the cross-linking between the polymeric chains is obtained in a template-free synthesis via complexation between anion and cation both present along the main chain (P(CMVImBr1.03-co-AA)); in this case, the reported CO_2 adsorption at 1 bar and 273 K was 0.64 mmol/g.[66] Other two works are also noteworthy, reporting silica supported tetraalkylammonium PILs (SiO_2-$P(VBTMA)(BF_4)$) and linear main-chain anionic PILs, having 1-butyl-3-methylimidazolium as counteraion (PUA-02), both reporting a maximum carbon dioxide adsorption of around 0.4 mmol/g at 1 bar and at 303 and 298K respectively.[67, 68] Another recent work, dealing with cross-linked di-vinylimidazolium PILs (PDMBr), reports CO_2 adsorption values of 1.02 mmol/g at 1 bar and 273 K ,[69] whereas the study by Talapaneni *et al.* dealing with imidazolium porous polymer obtained by a two-step synthesis (NP-imidazolium) reports adsorption of 1.74 mmol/CO_2 at 1 bar and 273 K.[7] This material is very similar to our CB-PCPs having equal SSA, but it has two more phenyl rings connecting every imidazolium moiety, slightly decreasing the ratio between

the imidazolium functional group and the aryl chain and, as a consequence, slightly decreasing the CO_2 loading.

In order to allow the comparison with the data reported in the literature, the isotherms of CO_2 uptake on CB-PCPs have been reported in mmol of carbon dioxide adsorbed per gram of each material (see Figure 6). However, to disclose information from the molecular point of view about the CO_2 adsorption, it is more relevant to take into consideration the mol% of carbon dioxide adsorbed with respect to the imidazolium moiety, as showed in Figure S13. From these isotherms, in fact, it is clear that the CO_2 uptake depends on the nature of the anion of the CB-PCPs. A previous study reports a higher CO_2 adsorption for PILs with acetate anion with respect to other anions and,[70] furthermore, some speculations were reported about a possible generation of imidazolium NHC upon heating and outgassing acetate PILs.[71, 72] Whereas, in the present case, CB-PCP 1 bearing the acetate anionshows the lowest performance towards CO_2 adsorption, if expressed in mol%. Usually, inorganic anion such as PF_6^- or BF_4^-, perform better than Tf_2N^- and TfO^- towards CO_2 adsorption for PILs developed in linear fashion.[70, 73] However, for cross-linked porous PILs, the Tf_2N^- anion shows the best performance.[48, 65] Generally speaking, it is difficult to discriminate among the effect of the anion nature, the SSA value and the polymer structure in carbon dioxide capture, due to the complexity of the adsorption process in which the chemical interaction, the diffusion kinetics inside the polymer network and the steric hindrance of the anion have to be considered. In agreement with the data already reported for porous PILs, the CO_2 adsorption by CB-PCPs follows thistrend: $Tf_2N^- > PF_6^- \approx TfO^- > BF_4^- > AcO^-$.

In comparison to other materials for CO_2 capture, our CB-PCPs exhibit better adsorption properties with respect to activated carbon, polycarbazole (PCBZ),[74] porous polymer network (PPN-80),[75] hypercrosslinked polymer (HCP-1)[76] and can compete with common porous aromatic framework (PAF-1).[77] Nevertheless, CB-PCPs still show less CO_2 uptake than the top performer materials like zeolitic imidazolate framework (ZIF-78),[78] zeolitic tetrazolate framework (ZTF-1)[79], zeolite 13X (ZEO13X),[80] and many metal organic framework.[81-83] Table 2 summarize the CO_2 adsorption at 1 bar for poly(ionic liquid)s and other kind of materials discussed in the text, in order to have a direct comparison of these sorbents with respect to CB-PCPs.

Table 2. Carbon dioxide adsorption performances of various selected materials

Sorbent	CO_2 mmol·g^{-1}	Conditions (P, T)	Ref.
Metal organic framework (Mg-MOF-74)	8.02	1 bar, 298 K	83
Zeolitic tetrazolate framework (ZTF-1)	5.59	1 bar, 273 K	79
Metal organic framework (UTSA-16)	4.90	1 bar, 273 K	82
Zeolite 13X (ZEO13X)	4.68	1 bar, 298 K	80
Zeolitic imidazolate framework (ZIF-78)	3.34	1 bar, 273 K	78
Click-based porous cationic polymer (CB-PCP-1)	2.05	1 bar, 273 K	this work
Porous aromatic framework (PAF-1)	2.05	1 bar, 273 K	77
Poly(ionic liquid) NP-imidazolium	1.74	1 bar, 273 K	7
Hypercrosslinked polymer (HCP-1)	1.70	1 bar, 298 K	76
Porous polymer network (PPN-80)	1.62	1 bar, 295 K	75
Polycarbazole (PCBZ)	1.13	1 bar, 273 K	74
Poly(ionic liquid) (PDMBr)	1.02	1 bar, 273 K	69
Poly(ionic liquid) P(CMVImBr1.03-co-AA)	0.64	1 bar, 273 K	66
Poly(ionic liquid) P(SVImTf2N)	0.46	1 bar, 273 K	65
Silica-poly(ionic liquid) (SiO_2-P(VBTMA)(BF_4))	0.40	1 bar, 303 K	67
Poly(ionic liquid) (PUA-02)	0.40	1 bar, 298 K	68

Generally speaking, good performances towards CO_2 adsorption in porous polymers are obtained from the combination of high surface area, microporosity, and high concentration of imidazolium active sites along the polymeric backbone. Furthermore, being the anion an integrating part of the adsorption properties of these materials, its choice is not straightforward, but depends on the chemical and morphological structure of the polymeric backbone. The weight ratio between the imidazolium moiety and the other parts of the polymer chemical structure is remarkable and this value is very high in our CB-PCPs. Furthermore, the direct conjugation of the imidazolium ring with two phenyl groups can change the distribution of its positive charge, so affecting the way in which the imidazolium moiety interacts with CO_2. It is worth noticing that, even though the CB-PCPs have about one tenth of the SSA of PAF-1 (5640 m^2/g),[15] they show very similar CO_2 capture capacities, testifying the relevance of the introduction of highly dispersed and accessible functional groups. In order to evaluate the effect of the porosity of CB-PCPs on carbon dioxide loading, the CO_2 adsorption at 298 k and 1 bar has been performed also on morphologically different samples **1a** and **1b**. The adsorption isotherms are reported in Figure S14. Sample **1** and **1a** exhibit exactly the same CO_2 loading of 1.2 mmol/g at 1 bar, moreover, sample **1a** shows a less pronounced hysteresis, probably due to the higher uniformity of the material in terms of microporosity.

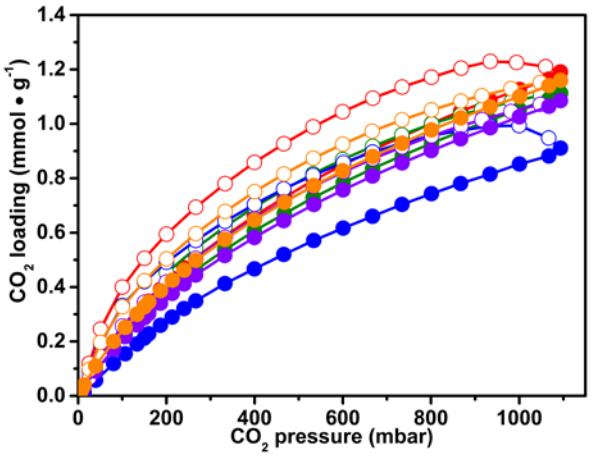

Figure 6. Carbon dioxide adsorption isotherm at 298 K for samples: **1** (red curve), **2** (blue curve), **3** (green curve), **4** (orange curve), **5** (violet curve). Spheres describes the adsorption branch, while circle describe the desorption branch.

Sample **1b,** with almost null SSA (see Figure S7 and Table 1), shows, however, a good adsorption capacity towards CO_2, with a maximum loading of 1 mmol/g. In fact, CO_2 can act as plasticizer for PILs, penetrate in part the bulk structure of non-porous polymers in a long diffusion time.[84, 85] For this reason, it is clear that the nature of the anions is more relevant than SSA in determining the CO_2 adsorption capacities of these materials.

1.1.5. *Carbon dioxide capture in presence of the carbene moiety*

It is well-known that, by means of strong organic bases, it is possible to introduce N-heterocyclic carbene in the C2 position of the imidazolium ring.[86-88] This carbene, in turn, can react with CO_2 forming a new C-C bond and a carboxylate species directly linked to the imidazolium ring. The so formed imidazolium carboxilate is thermally unstable and can decompose below 100 °C releasing CO_2 and restoring the carbene, which can restart the adsorption/desorption cycle.[89-91] The overall process is reported in Scheme 2. The chemical looping is considered as a new frontier in carbon dioxide adsorption.[92] This mechanism was already studied for different ionic liquids and poly(ionic liquid)s, as a way for storing CO_2 and also protecting the carbene from the decomposition in the presence of moisture.[7, 66, 89, 90, 93-97]

In our study, we direct the efforts to unravel the differences, from the physico-chemical point of view, between the CO_2 capture by means of the as-synthesized CB-PCPs and the CB-PCPs bearing the NHC. A direct comparison between the CO_2 adsorption capacity at 298 K of the CB-PCP bearing the NHC (sample **6**) and of its precursor (sample **1**) is reported in Figure 7. The maximum CO_2 loading of sample **6** is 1.1 mmol/g, a perfectly comparable value with the uptake reported for sample **1**. Conversely, from a molecular point of view, data reported in mol% of CO_2 loading with respect to the imidazolium or the NHC moieties clearly show that the maximum loading drastically decreases after the introduction of the carbene (from 36 mol% for sample **1** to 26 mol% for sample **6**). This behavior is ascribable to the lower number of available active sites. In fact, when NHC carbene moieties are formed, their reactivity favour the coupling.. This phenomenon is also responsible for the evident decrease of the SSA of sample **6** (see Table 1). The dimers, without free electronic doublet, are not chemically able to bond CO_2, thus decreasing the overall adsorption capacity with respect to the imidazolium moiety. However, the lightness of sample **6**, arising from a lower molecular weight of the monomeric unit, compensates the loss of active sites, giving the same performance in terms of CO_2 loading per mass unit of adsorbent.

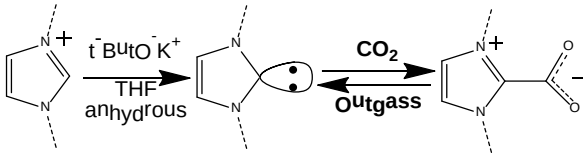

Scheme 2. Synthetic step for the introduction of carbene in the imidazolium ring (left side) and reversible formation of the NHC-CO_2 adduct (right side).

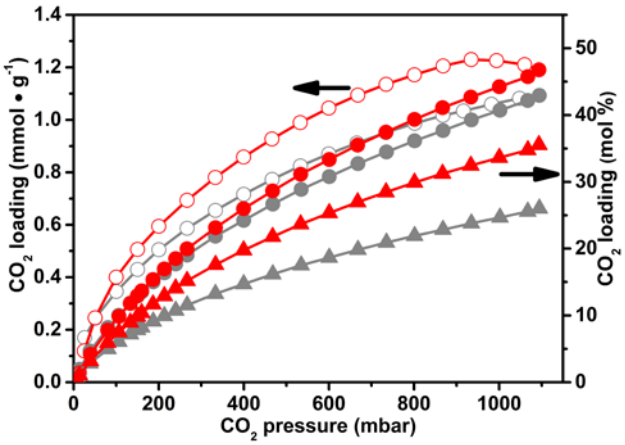

Figure 7. Carbon dioxide adsorption isotherm at 298 K for sample **1** and **6**. Spheres and circle describes respectively the adsorption and branch referring to the scale on the left (mmol/g), while triangles of adsorption branch refers to to the scale on the right (mol% of CO_2 respect to the imidazolium or NHC moieties).

In-situ FTIR spectroscopy was used to follow the reaction between the polymer bearing NHC and carbon dioxide. The effect of CO_2 contact on the pre-activated sample **6**, is illustrated in Figure 8. The IR spectrum of sample **6** after activation (black curve) is characterized by the spectral features of the polymeric framework. Upon 1 h contact with 200 mbar of CO_2, two new bands appear in the spectrum at 1665 cm^{-1} and at 1295 cm^{-1} (dark grey curve), ascribable to the $\nu_{asym}(OCO^-)$ and the $\nu_{sym}(OCO^-)$ of the formed imidazolium carboxylate.[66, 89, 98, 99] The formation of a carboxilate species testifies the activation of carbon dioxide, as proved by the deep change in its molecular orbitals.[100] It is worth noticing that, after the CO_2 contact, the evacuation

at beam temperature (around 50 °C) (light grey curve) almost restore the spectrum of the material after activation. The same experiment was repeated for sample **1** without any evidence of carboxylate formation upon exposure of the CB-PCP to 200 mbar of CO_2.

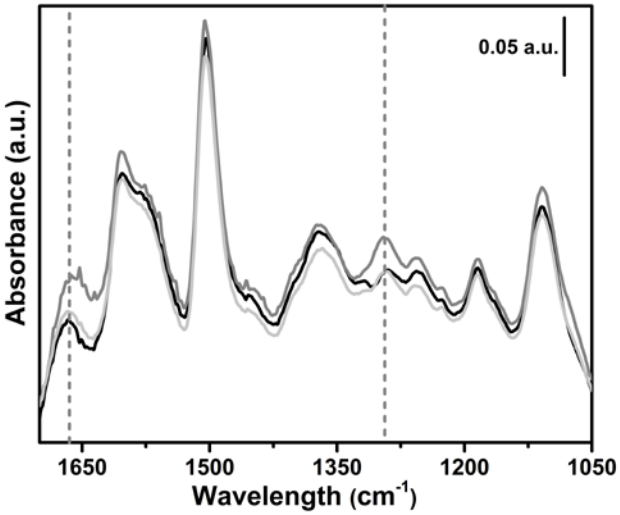

Figure 8. *In-situ* FTIR spectra upon dosage of 200 mbar carbon dioxide on sample **6**. Black curve: activated sample. Dark grey curve: 1 h contact with 200 mbar of CO_2. Light grey curve: CO_2 evacuation.

Micro-calorimetric gas adsorption experiments were performed to further investigate the interaction energy between CO_2, the ionic CB-PCP and its carbene counterpart. The differential molar adsorption heats of samples **1** and **6** are reported in Figure **9** as a function of the carbon dioxide coverage, whereas their corresponding quantitative and calorimetric isotherms are shown in Figure S15 and S16 respectively. In the case of sample **1,** the differential heat of adsorption at zero coverage is 35 KJ/mol, then it decreases to 10 KJ/mol for higher CO_2 coverages, *i.e.* significantly under the value of CO_2 molar liquefaction enthalpy. This low isosteric heat could be explained considering two overlaying contributions: the gas adsorption and the structure rearrangement as a consequence of the polymer swelling process.[66] Conversely, for sample **6** the differential heat of adsorption is definitely higher, starting from 58 KJ/mol at low coverage and decreasing to about 35-40 KJ/mol at high coverage. The higher differential heat of interaction of sample **6** is perfectly in line with the formation of the adduct between the NHC and CO_2. Still, the comparison between the primary (spheres) and secondary (circles) runs indicates that the CO_2 uptake is mostly reversible also for samples **6**.

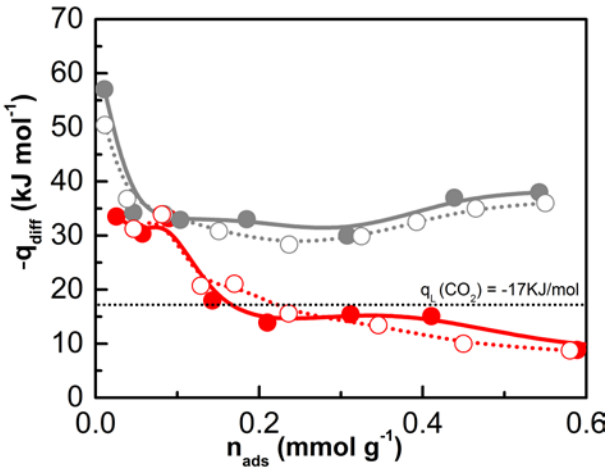

Figure 9. Differential molar adsorption heatsas a function of the coverage relative to the adsorption at 298 K of CO_2 on samples **1** (red curves) and **6** (grey curves). Spheres refer to the primary adsorption adsorption and circles to the secondary ones. The dotted horizontal line represents the standard molar enthalpy of liquefaction of CO_2 at 298K.

Conclusions

We described a facile and straightforward synthetic way to obtain click reaction-based micro-/mesoporous cationic polymers. A set of materials with different anions was successfully synthesized and characterized in order to confirm their structure and to study their porosity. It was demonstrated that CB-PCPs exhibit an excellent behavior towards carbon dioxide adsorption, either at 298 K and 1 bar, with a CO_2 loading above 1 mmol/g for all the samples, or even more at 273K and 1 bar where the loading for CB-PCP **1** is 2 mmol/g, achieving the highest value for porous ionic polymer. CB-PCP **1** was also modified in order to introduce the NHC on the imidazolium ring. The performances towards carbon dioxide adsorption of the NHC CB-PCP are of the same level of those of the ionic CB-PCPs, even though they show a different adsorption mechanism. The combination of *in-situ* FTIR spectroscopy and of adsorption micro-calorimetry reveals two adsorption processes of completely different nature: on one hand, a plain physisorption process in the ionic CB-PCPs and, on the other hand, the chemisorption of carbon dioxide in the NHC polymer.

Acknowledgements

Thanks are due to Prof. Leonardo Marchese and Geo Paul (Università del Piemonte Orientale "A. Avogadro") for SS-NMR measurements and the useful discussions.

Funding Sources

Italian Ministry of University and Research (MIUR). Project PRIN 2010-2011 n:2010A2FSS9.
ERC (European Research Council) Starting Grant. Project number 639720 – NAPOLI

References

1. A. G. Slater and A. I. Cooper, *Science*, 2015, **348**.
2. Y. Xu, S. Jin, H. Xu, A. Nagai and D. Jiang, *Chem. Soc. Rev.*, 2013, **42**, 8012-8031.
3. A. I. Cooper, *Adv. Mater.*, 2009, **21**, 1291-1295.
4. T. Ben and S. Qiu, *CrystEngComm*, 2013, **15**, 17-26.
5. J.-K. Sun, M. Antonietti and J. Yuan, *Chem. Soc. Rev.*, 2016, DOI: 10.1039/C6CS00597G.
6. H. Ren, T. Ben, E. Wang, X. Jing, M. Xue, B. Liu, Y. Cui, S. Qiu and G. Zhu, *Chem. Commun.*, 2010, **46**, 291-293.
7. S. N. Talapaneni, O. Buyukcakir, S. H. Je, S. Srinivasan, Y. Seo, K. Polychronopoulou and A. Coskun, *Chem. Mater.*, 2015, **27**, 6818-6826.
8. Y. Yuan, F. Sun, H. Ren, X. Jing, W. Wang, H. Ma, H. Zhao and G. Zhu, *J. Mater. Chem.*, 2011, **21**, 13498-13502.
9. H. Zhao, Z. Jin, H. Su, X. Jing, F. Sun and G. Zhu, *Chem. Commun.*, 2011, **47**, 6389-6391.
10. L. Chen, Y. Honsho, S. Seki and D. Jiang, *J. Am. Chem. Soc.*, 2010, **132**, 6742-6748.
11. T. Ben, K. Shi, Y. Cui, C. Pei, Y. Zuo, H. Guo, D. Zhang, J. Xu, F. Deng, Z. Tian and S. Qiu, *J. Mater. Chem.*, 2011, **21**, 18208-18214.
12. M. Rose, A. Notzon, M. Heitbaum, G. Nickerl, S. Paasch, E. Brunner, F. Glorius and S. Kaskel, *Chem. Commun.*, 2011, **47**, 4814-4816.
13. H. C. Cho, H. S. Lee, J. Chun, S. M. Lee, H. J. Kim and S. U. Son, *Chem. Commun.*, 2011, **47**, 917-919.
14. J.-X. Jiang, F. Su, A. Trewin, C. D. Wood, N. L. Campbell, H. Niu, C. Dickinson, A. Y. Ganin, M. J. Rosseinsky, Y. Z. Khimyak and A. I. Cooper, *Angew. Chem. Int. Ed.*, 2007, **46**, 8574-8578.
15. T. Ben, H. Ren, S. Ma, D. Cao, J. Lan, X. Jing, W. Wang, J. Xu, F. Deng, J. M. Simmons, S. Qiu and G. Zhu, *Angew. Chem.*, 2009, **121**, 9621-9624.
16. O. Buyukcakir, S. H. Je, D. S. Choi, S. N. Talapaneni, Y. Seo, Y. Jung, K. Polychronopoulou and A. Coskun, *Chem. Commun.*, 2016, **52**, 934-937.
17. A. Thomas, *Angew. Chem. Int. Ed.*, 2010, **49**, 8328-8344.
18. T. Muller and S. Brase, *RSC Adv.*, 2014, **4**, 6886-6907.
19. T. Muller and S. Bräse, *Angew. Chem. Int. Ed.*, 2011, **50**, 11844-11845.
20. P. Rekha, U. Sahoo and P. Mohanty, *RSC Adv.*, 2014, **4**, 34860-34863.
21. J. R. Holst, E. Stöckel, D. J. Adams and A. I. Cooper, *Macromolecules*, 2010, **43**, 8531-8538.
22. P. Pandey, O. K. Farha, A. M. Spokoyny, C. A. Mirkin, M. G. Kanatzidis, J. T. Hupp and S. T. Nguyen, *J. Mater. Chem.*, 2011, **21**, 1700-1703.
23. O. Plietzsch, C. I. Schilling, T. Grab, S. L. Grage, A. S. Ulrich, A. Comotti, P. Sozzani, T. Muller and S. Brase, *New J. Chem.*, 2011, **35**, 1577-1581.
24. J. Yuan and M. Antonietti, *Polymer*, 2011, **52**, 1469-1482.
25. J. Yuan, D. Mecerreyes and M. Antonietti, *Prog. Polym. Sci.*, 2013, **38**, 1009-1036.
26. D. Mecerreyes, *Prog. Polym. Sci.*, 2011, **36**, 1629-1648.
27. J. Lu, F. Yan and J. Texter, *Prog. Polym. Sci.*, 2009, **34**, 431-448.
28. S. N. Riduan and Y. Zhang, *Chem. Soc. Rev.*, 2013, **42**, 9055-9070.
29. A. S. Shaplov, D. O. Ponkratov and Y. S. Vygodskii, *Polym. Sci. Ser. B*, 2016, **58**, 73-142.
30. A. Dani, E. Groppo, C. Barolo, J. G. Vitillo and S. Bordiga, *J. Mater. Chem. A*, 2015, **3**, 8508-8518.
31. J. Cui, W. Zhu, N. Gao, J. Li, H. Yang, Y. Jiang, P. Seidel, B. J. Ravoo and G. Li, *Angew. Chem. Int. Ed.*, 2014, **53**, 3844-3848.
32. Q. Zhao, P. Zhang, M. Antonietti and J. Yuan, *J. Am. Chem. Soc.*, 2012, **134**, 11852-11855.
33. F. Yan and J. Texter, *Angew. Chem. Int. Ed.*, 2007, **46**, 2440-2443.
34. H. Zhao, Y. Wang and R. Wang, *Chem. Commun.*, 2014, **50**, 10871-10874.
35. K. Thiel, R. Zehbe, J. Roeser, P. Strauch, S. Enthaler and A. Thomas, *Polym. Chem.*, 2013, **4**, 1848-1856.
36. H. C. Kolb, M. G. Finn and K. B. Sharpless, *Angew. Chem. Int. Ed.*, 2001, **40**, 2004-2021.
37. O. Mahmoodi Nosrat, I. Nikokar, M. Farhadi and A. Ghavidast, *Z. Naturforsch., B: Chem. Sci.*, 2014, **69**, 715.
38. H. Debus, *Justus Liebigs Ann. Chem.*, 1858, **107**, 199-208.
39. B. Radziszewski, *Ber. Dtsch. Chem. Ges.*, 1882, **15**, 1493-1496.
40. A. J. Arduengo, T. K. Prakasha, F. P. Gentry and H. E. Simmons, *WO2002040454 A1*, 2002.
41. D. Esposito, S. Kirchhecker and M. Antonietti, *Chem. Eur. J.*, 2013, **19**, 15097-15100.
42. J.-P. Lindner, *Macromolecules*, 2016, **49**, 2046-2053.

43. K.-S. Krannig, D. Esposito and M. Antonietti, *Macromolecules*, 2014, **47**, 2350-2353.
44. A. R. Hajipour and Z. Khorsandi, *Catal. Commun.*, 2016, **77**, 1-4.
45. W. Yu, Z. Wen-Li, C. Hao, Z. Li-Zhuo, Z. Qiu-Ju, Z. Huan, W. Yuan-Jiang, G. Wen-Hui, F. Yue, Z. Sheng-Liang and W. Hui, *Asian J. Chem.*, 2015, **27**, 3107-3110.
46. M. Lee, U. H. Choi, D. Salas-de la Cruz, A. Mittal, K. I. Winey, R. H. Colby and H. W. Gibson, *Adv. Funct. Mater.*, 2011, **21**, 708-717.
47. N. Matsumi, K. Sugai, M. Miyake and H. Ohno, *Macromolecules*, 2006, **39**, 6924-6927.
48. S. Zulfiqar, M. I. Sarwar and D. Mecerreyes, *Polym. Chem.*, 2015, **6**, 6435-6451.
49. M. Ramdin, T. W. de Loos and T. J. H. Vlugt, *Ind. Eng. Chem. Res.*, 2012, **51**, 8149-8177.
50. Y. Zhou, J. Liu, M. Xiao, Y. Meng and L. Sun, *ACS Appl. Mater. Interfaces*, 2016, **8**, 5547-5555.
51. R. Dawson, A. I. Cooper and D. J. Adams, *Polym. Int.*, 2013, **62**, 345-352.
52. B. M. Trost, *Angew. Chem. Int. Ed.*, 1995, **34**, 259-281.
53. N. B. Colthup, L. H. Daly and S. E. Wiberley, *Introduction to Infrared and Raman Spectroscopy (Third Edition)*, Academic Press, San Diego, 1990.
54. R. L. Frost and J. T. Kloprogge, *J. Mol. Struct.*, 2000, **526**, 131-141.
55. L. Yu, J. Clifford, T. T. Pham, E. Almaraz, F. Perry, G. A. Caputo and T. D. Vaden, *J. Phys. Chem. B*, 2013, **117**, 7057-7064.
56. R. Holomb, A. Martinelli, I. Albinsson, J. C. Lassègues, P. Johansson and P. Jacobsson, *J. Raman Spectrosc.*, 2008, **39**, 793-805.
57. H. Zine, M. H. Baron and A. Piart-Goypiron, *Spectrochim. Acta Mol. Biomol. Spectrosc.*, 1995, **51**, 457-470.
58. N. N. Sa'adun, R. Subramaniam and R. Kasi, *Scientific World J.*, 2014, **2014**, 7.
59. Y. Kaneko, M. Shoiriki and T. Mizumo, *J. Mater. Chem.*, 2012, **22**, 14475-14478.
60. M. L. Pinto, L. Mafra, J. M. Guil, J. Pires and J. Rocha, *Chem. Mater.*, 2011, **23**, 1387-1395.
61. M. M. Cecchini, J. Steinkoenig, S. Reale, L. Barner, J. Yuan, A. S. Goldmann, F. De Angelis and C. Barner-Kowollik, *Chem. Sci.*, 2016, **7**, 4912-4921.
62. J. Weber, M. Antonietti and A. Thomas, *Macromolecules*, 2008, **41**, 2880-2885.
63. J. Weber and A. Thomas, *J. Am. Chem. Soc.*, 2008, **130**, 6334-6335.
64. F. E. Hahn, L. Wittenbecher, D. Le Van and R. Fröhlich, *Angew. Chem. Int. Ed.*, 2000, **39**, 541-544.
65. A. Wilke, J. Yuan, M. Antonietti and J. Weber, *ACS Macro Lett.*, 2012, **1**, 1028-1031.
66. S. Soll, Q. Zhao, J. Weber and J. Yuan, *Chem. Mater.*, 2013, **25**, 3003-3010.
67. H. Cheng, P. Wang, J. Luo, J. Fransaer, D. E. De Vos and Z.-H. Luo, *Ind. Eng. Chem. Res.*, 2015, **54**, 3107-3115.
68. T. O. Magalhaes, A. S. Aquino, F. D. Vecchia, F. L. Bernard, M. Seferin, S. C. Menezes, R. Ligabue and S. Einloft, *RSC Adv.*, 2014, **4**, 18164-18170.
69. X. Wang, Y. Zhou, Z. Guo, G. Chen, J. Li, Y. Shi, Y. Liu and J. Wang, *Chem. Sci.*, 2015, **6**, 6916-6924.
70. E. I. Privalova, E. Karjalainen, M. Nurmi, P. Mäki-Arvela, K. Eränen, H. Tenhu, D. Y. Murzin and J.-P. Mikkola, *ChemSusChem*, 2013, **6**, 1500-1509.
71. G. Gurau, H. Rodríguez, S. P. Kelley, P. Janiczek, R. S. Kalb and R. D. Rogers, *Angew. Chem. Int. Ed.*, 2011, **50**, 12024-12026.
72. J. Blath, N. Deubler, T. Hirth and T. Schiestel, *Chem. Eng. J.*, 2012, **181–182**, 152-158.
73. J. Tang, H. Tang, W. Sun, M. Radosz and Y. Shen, *J. Polym. Sci., Part A: Polym. Chem.*, 2005, **43**, 5477-5489.
74. M. Saleh, S. B. Baek, H. M. Lee and K. S. Kim, *J. Phys. Chem. C*, 2015, **119**, 5395-5402.
75. L.-B. Sun, A.-G. Li, X.-D. Liu, X.-Q. Liu, D. Feng, W. Lu, D. Yuan and H.-C. Zhou, *J. Mater. Chem. A*, 2015, **3**, 3252-3256.
76. C. F. Martin, E. Stockel, R. Clowes, D. J. Adams, A. I. Cooper, J. J. Pis, F. Rubiera and C. Pevida, *J. Mater. Chem.*, 2011, **21**, 5475-5483.
77. T. Ben, C. Pei, D. Zhang, J. Xu, F. Deng, X. Jing and S. Qiu, *Energy Environ. Sci.*, 2011, **4**, 3991-3999.
78. R. Banerjee, H. Furukawa, D. Britt, C. Knobler, M. O'Keeffe and O. M. Yaghi, *J. Am. Chem. Soc.*, 2009, **131**, 3875-3877.
79. T. Panda, P. Pachfule, Y. Chen, J. Jiang and R. Banerjee, *Chem. Commun.*, 2011, **47**, 2011-2013.
80. D. P. Bezerra, R. S. Oliveira, R. S. Vieira, C. L. Cavalcante and D. C. S. Azevedo, *Adsorption*, 2011, **17**, 235-246.
81. K. Sumida, D. L. Rogow, J. A. Mason, T. M. McDonald, E. D. Bloch, Z. R. Herm, T.-H. Bae and J. R. Long, *Chem. Rev.*, 2012, **112**, 724-781.

82. A. Masala, F. Grifasi, C. Atzori, J. G. Vitillo, L. Mino, F. Bonino, M. R. Chierotti and S. Bordiga, *J. Phys. Chem. C*, 2016, **120**, 12068-12074.
83. J. A. Mason, K. Sumida, Z. R. Herm, R. Krishna and J. R. Long, *Energy Environ. Sci.*, 2011, **4**, 3030-3040.
84. J. Tang, W. Sun, H. Tang, M. Radosz and Y. Shen, *Macromolecules*, 2005, **38**, 2037-2039.
85. J. Tang, H. Tang, W. Sun, H. Plancher, M. Radosz and Y. Shen, *Chem. Commun.*, 2005, DOI: 10.1039/B501940K, 3325-3327.
86. A. J. Arduengo, R. L. Harlow and M. Kline, *J. Am. Chem. Soc.*, 1991, **113**, 361-363.
87. M. N. Hopkinson, C. Richter, M. Schedler and F. Glorius, *Nature*, 2014, **510**, 485-496.
88. M. Fevre, J. Pinaud, Y. Gnanou, J. Vignolle and D. Taton, *Chem. Soc. Rev.*, 2013, **42**, 2142-2172.
89. B. R. Van Ausdall, J. L. Glass, K. M. Wiggins, A. M. Aarif and J. Louie, *J. Org. Chem.*, 2009, **74**, 7935-7942.
90. H. Zhou, W.-Z. Zhang, Y.-M. Wang, J.-P. Qu and X.-B. Lu, *Macromolecules*, 2009, **42**, 5419-5421.
91. L. Yang and H. Wang, *ChemSusChem*, 2014, **7**, 962-998.
92. T. M. McDonald, J. A. Mason, X. Kong, E. D. Bloch, D. Gygi, A. Dani, V. Crocella, F. Giordanino, S. O. Odoh, W. S. Drisdell, B. Vlaisavljevich, A. L. Dzubak, R. Poloni, S. K. Schnell, N. Planas, K. Lee, T. Pascal, L. F. Wan, D. Prendergast, J. B. Neaton, B. Smit, J. B. Kortright, L. Gagliardi, S. Bordiga, J. A. Reimer and J. R. Long, *Nature*, 2015, **519**, 303-308.
93. M. Fèvre, P. Coupillaud, K. Miqueu, J.-M. Sotiropoulos, J. Vignolle and D. Taton, *J. Org. Chem.*, 2012, **77**, 10135-10144.
94. J. Pinaud, J. Vignolle, Y. Gnanou and D. Taton, *Macromolecules*, 2011, **44**, 1900-1908.
95. G. W. Nyce, J. A. Lamboy, E. F. Connor, R. M. Waymouth and J. L. Hedrick, *Org. Lett.*, 2002, **4**, 3587-3590.
96. M. Hans, L. Delaude, J. Rodriguez and Y. Coquerel, *J. Org. Chem.*, 2014, **79**, 2758-2764.
97. R. Lambert, P. Coupillaud, A.-L. Wirotius, J. Vignolle and D. Taton, *Macromol. Rapid Commun.*, 2016, **37**, 1143-1149.
98. J. Oomens and J. D. Steill, *J. Phys. Chem. A*, 2008, **112**, 3281-3283.
99. P. M. MacQueen, R. A. Bach, C. T. P. MacLean and S. L. MacQuarrie, *J. Phys. Chem. C*, 2014, **118**, 5239-5242.
100. H. J. Freund and M. W. Roberts, *Surf. Sci. Rep.*, 1996, **25**, 225-273.